

Study of the Effects of Hydroxyapatite Nanocrystal Codoping by Pulsed Electron Paramagnetic Resonance Methods

M. R. Gafurov^{a,*}, T. B. Biktagirov^a, G. V. Mamin^a, D. V. Shurtakova^a,
E. S. Klimashina^b, V. I. Putlyaev^b, and S. B. Orlinskii^a

^a Kazan Federal University, ul. Kremlevskaya 18, Kazan, 420008 Tatarstan, Russia

^b Moscow State University, Moscow, 119992 Russia

*e-mail: marat.gafurov@kpfu.ru

Received July 13, 2015

Abstract—The effect of codoping of hydroxyapatite (HAP) nanocrystals with average sizes of 35 ± 15 nm during “wet” synthesis by CO_3^{2-} carbonate anions and Mn^{2+} cations on relaxation characteristics (for the times of electron spin–spin relaxation) of the NO_3^{2-} nitrate radical anion has been studied. By the example of HAP, it has been demonstrated that the electron paramagnetic resonance (EPR) is an efficient method for studying anion–cation (co)doping of nanoscale particles. It has been shown experimentally and by quantum-mechanical calculations that simultaneous introduction of several ions can be energetically more favorable than their separate inclusion. Possible codoping models have been proposed, and their energy parameters have been calculated.

DOI: 10.1134/S1063783416030094

1. INTRODUCTION

Positive effects of codoping of source materials with various ions on properties of laser and semiconductor crystals are studied in sufficient detail experimentally and theoretically. Optimally selected codoping parameters can lead to a significant increase in the radiation energy yield of laser crystals; an increase in the stability of a number of their physical characteristics to light, radiation, and other external factors make it possible to suppress or increase crystal afterglow by several orders of magnitude, affect mechanical properties, and others [1–3]. Nevertheless, the study of the effects of nanosystems doping and codoping is still in its infancy.

In recent decades, indefatigable interest has been given to hydroxyapatite (HAP) $\text{Ca}_{10}(\text{PO}_4)_6(\text{OH})_2$ materials modified by various ions [4]. Synthetic HAP (apart from that it is an ideal model material for studying osteointegration processes, i.e., the interactions of an implant with a native bone) features a broad spectrum of potential and already implemented applications in instrument engineering (sorbents, lumino-phores, piezoelectrics) and for biomedical applications (materials for bone tissue implantation, targeted delivery of fluorescent preparations, contrast agents, and drugs to tissues under study, sorbents of heavy metals and radio nuclides, and others) [5, 6]. The literature mentions the possibility of using HAP as a highly efficient absorber of nitrates from soil and sub-

soil waters [7], substrate for catalysts [8], and more. Selective antitumorous activity of HAP nanocrystals was recently shown in [9, 10].

Despite the large number of the studies performed, many important problems relating to anionic and cationic substitutions in HAP have not been studied in sufficient detail, and data of many studies are contradictory. In this respect, apatite continues to justify its name which in the translation from Greek means “mislead.” The most contradictive information is associated with the type of defects appearing during doping, impurity localization sites in biomineral and synthetic samples and the nanoparticle doping possibility itself; the extended nanocrystal surface controls the radically different thermodynamics of impurity ion introduction. We note that some impurities cause cytotoxicity and lead to material rejection by organisms. It is clear that among such impurities are, in particular, the NO_3^- nitrate anion, taking into account that the main HAP synthesis method is precipitation from nitrate salt solutions.

The problems of HAP nanoparticle codoping only recently began to attract close attention from some research groups. The effect of simultaneous substitution with various ions and groups on physicochemical properties of materials and the possibility itself of such codoping during nanoparticle synthesis is almost unstudied, and corresponding analytical approaches have not been developed. To our knowledge, there are

only a few works on this subject [11, 12]: anion–cation codoping Mg^{2+} and CO_3^{2-} , Zn^{2+} and CO_3^{2-} , Sr^{2+} and CO_3^{2-} , and cation–cation codoping (Mg^{2+} , Sr^{2+} , and Mn^{2+}).

In a number of our recent works [13–19], we demonstrated that the use of some modern commercially implemented approaches of the electron paramagnetic resonance (EPR) makes it possible to significantly extend the ranges of the study of the HAP composition and structure, and nanoscale HAP of both synthetic and biogenic origin [5, 20, 21]. In [16], we showed how spectroscopic characteristics of radiation-induced nitrogen centers NO_3^{2-} introduced initially as nitrates as an undesirable impurity during “wet” synthesis change with the introduction of CO_3^{2-} carbonate ions. It was demonstrated that anion–anion codoping and substitution can be studied using NO_3^{2-} centers as an EPR probe. In this work, spectroscopic and relaxation characteristics of the nitrate radical during HAP nanocrystal codoping with carbonate ions and Mn^{2+} cations were studied. Using the example of nanoscale HAP powders, it is shown that the EPR method can be an efficient means for studying anion and cation (co)doping.

2. MATERIALS AND METHODS

Nanocrystalline HAP powders, namely $\text{Ca}_{10}(\text{PO}_4)_6(\text{OH})_2$ (“pure” HAP), $\text{Ca}_{10-x}\text{Na}_x(\text{PO}_4)_{6-x}(\text{CO}_3)_x(\text{OH})_2$ (CO–HAP), and $\text{Ca}_{10-y}\text{Mn}_y(\text{PO}_4)_6(\text{OH})_2$ (Mn–HAP) with average crystallite sizes from 20 to 50 nm and x and y from 0 to 2 and from 0 to 0.5, respectively, were synthesized by precipitation from an aqueous solution. Calcium nitrate monohydrate $\text{Ca}(\text{NO}_3)_2 \cdot \text{H}_2\text{O}$ (235 g) was dissolved in 420 mL 20 wt % NH_4OH (solution A), while $(\text{NH}_4)_2\text{HPO}_4$ (72.2 g) was dissolved in 380 mL deionized water (solution B). 30 mL 20 wt % NH_4OH were added after complete $(\text{NH}_4)_2\text{HPO}_4$ dissolution. A required stoichiometric $\text{MnSO}_4 \cdot \text{H}_2\text{O}$ amount was dissolved in 100 mL of deionized water, added to solution A, and mixed for 5 min. Then solution B was added to solution A under strong stirring using a magnetic mixer and was kept for 24 h. The obtained precipitates were aged for 48 h and then were decanted and washed by 2.5 L of deionized water three times to remove the accompanying product of the reaction between NH_4OH and NO_3^- . The precipitate was washed three times and then was filtered by a Buchner funnel. Mn–HAP precipitates were annealed at a temperature of 900°C for 3 h to improve the degree of crystallinity and to additionally remove NH_4OH . Procedures of synthesis of samples of pure HAP and CO–HAP and details of chemical and heat treatment of samples with the purpose of achieving the highest degree of crystallinity and purification of a final prod-

uct from foreign impurities are given in our previous studies [13, 16, 17].

The prepared samples were characterized by the methods of electron microscopy (LEO SUPRA 50VP, Carl Zeiss, 5 kV), X-ray diffraction analysis (Rigaku D/MAX 2500 with a rotating anode and Bruker D2 Phaser), local electron probe microanalysis (INCA Energy+ combined with –LEO SUPRA 50VP), infrared spectroscopy (Perkin-Elmer 1600), inductively coupled plasma mass spectrometry (ICP-MS, Perkin Elmer, ELAN–DRC II).

No EPR signals from “pure” HAP and CO–HAP samples were observed. To produce paramagnetic complex of materials under study, samples were irradiated with X-rays at room temperature using an URS-55 setup ($U = 55$ kV, $I = 16$ mA, W anticathode). The irradiation dose was ~ 10 kGy. The EPR spectra were studied at the X -range (9.6 GHz) Elexsys 580 (Bruker) spectrometer of the shared service center of physicochemical studies of the Kazan Federal University (KFU), using steady and pulsed modes. In the pulsed mode, conventional two- and three-pulse trains were used [22]. Electron spin echo (ESE) was measured using the $\pi/2$ – τ – π sequence, where the pulse duration π was 16 ns, and the time delay was $\tau = 240$ ns. To measure the phase memory time (transverse relax-

ation time, T_2^*), the duration τ was varied with a minimum step of 4 ns. To measure the spin–lattice (longitudinal) relaxation time T_1 , the inversion–recovery sequence τ – T_{delay} – $\pi/2$ – τ – π was used, where the time delay T_{delay} was varied, while τ was fixed. The study was conducted in the temperature range from 20 to 300 K. Samples were studied before and after X-ray irradiation.

The quantum-chemical study of the interaction of impurity centers in the HAP crystal was performed within the density functional theory (DFT) in the spin-polarized formalism using the generalized gradient approximation in the PBE version [23] for the exchange–correlation functional and Vanderbilt pseudopotentials [24]. The boundary value of the kinetic energy of plane waves was chosen as 40 Ry, while the electron density did not exceed 320 Ry. The strongly correlated $3d$ -shell of the Mn^{2+} ions was described using the local Coulomb interaction U (DFT + U method). The corrections U in the Hubbard model formalism was chosen as 3 eV using the linear response method [25].

All calculations were performed using the Quantum Espresso package [26]. The calculation details, descriptions of the HAP structure and the used model of a nitrogen-containing impurity are given in our previous papers [16–18]. According to [16–18], the NO_3^- ion (hence, the NO_3^{2-} radical) in the HAP structure substitutes the orthophosphate group, and the charge is compensated by removing one of neighboring Ca

atoms. The Ca vacancy site was chosen such that to provide the lowest ground state energy of the calculated HAP cell containing no Mn^{2+} ions. Then impurity Mn^{2+} ions substituting Ca^{2+} ions were introduced into the cell. The calculated HAP cell consisted of 88 atoms (in the absence of impurities). Three configurations with various relative positions of NO_3^{2-} and Mn^{2+} impurities with interatomic distances $r_{\text{N-Mn}} = 0.34, 0.63, \text{ and } 0.85$ nm were considered. For each configuration, the value of the scalar exchange interaction between paramagnetic centers was determined, which is described by the Hamiltonian

$$H = -J_{\text{ex}} S_{\text{Mn}} S_{\text{N}}, \quad (1)$$

where S_{Mn} and S_{N} are the operators of manganese ion and radical spins. The constant J_{ex} was determined based on the results of DFT + U calculations,

$$J_{\text{ex}} = (E_{\text{LS}} - E_{\text{HS}}) / S_{\text{max}} (S_{\text{max}} + 1), \quad (2)$$

where E_{HS} and E_{LS} are the system ground state energies calculated for high-spin and low-spin configurations, respectively; $S_{\text{max}} = |S_{\text{Mn}}| + |S_{\text{N}}| = 3$ (see [27]).

3. RESULTS

Before X-ray irradiation of Mn-HAP samples, their W -band (95 GHz) spectrum exhibited the typical 6-component EPR powder spectrum of Mn^{2+} ions with $g = 2.001(1)$ and the hyperfine interaction constant $A = 9.1(2)$ mT (see our paper [15]). The Mn^{2+} spectrum was unchanged upon annealing to temperatures of $\sim 900^\circ\text{C}$, which can be considered as the indication of preferential localization of Mn^{2+} ions in the HAP nanocrystal bulk. In the X -band, the manganese EPR spectrum represents a broad unsolved line (see below). The EPR spectra of nitrogen-containing and carbonate radicals were not detected, as well as other EPR lines.

The EPR spectrum of the irradiated Mn-HAP sample is shown in Fig. 1. We can see that the characteristic nitrate radical signal caused by the hyperfine interaction with the nuclear magnetic moment of the ^{14}N nucleus ($I = 1$) is added to the Mn^{2+} signal (broad one) in the EPR spectrum. The nitrate signal nature, EPR line shape, spectroscopic characteristics, and changes in the nitrate radical spectrum in the case of HAP doping with carbonate ions are considered in detail in [16, 17, 19].

The magnetic field in which relaxation characteristics were measured corresponds to the perpendicular component of the nitrogen radical g -factor g_{\perp} (the electron spin echo signal maximum, see Fig. 1). As follows from the inset in Fig. 1 ($T = 100$ K), Fig. 2 ($T = 300$ K), and the table, the measured relaxation characteristics differ significantly depending on the sample impurity composition. While the introduction of carbonate ions does not affect the relaxation parameters

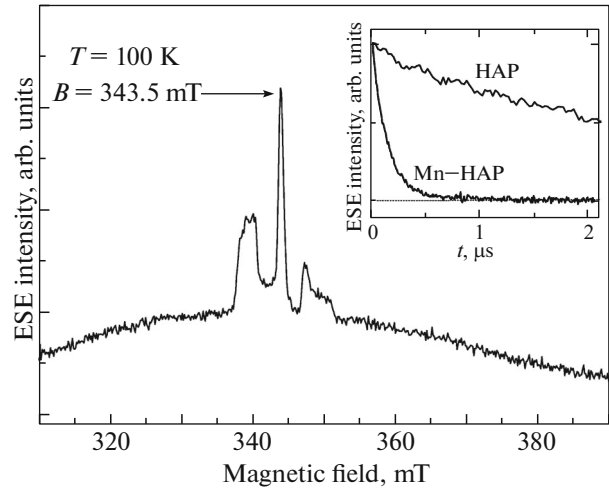


Fig. 1. Echo-detected EPR spectra of Mn-HAP nanocrystals ($y = 0.05$) at $T = 100$ K after exposure to X-ray radiation; the inset illustrates the effect of HAP sample codoping with manganese ions on transverse magnetization decay for the NO_3^{2-} center at $T = 100$ K. The magnetic field in which relaxation characteristics of the NO_3^{2-} radical measurements in all samples under study is done indicated by an arrow.

T_1 and T_2^* of the nitrate ion, the introduction of Mn^{2+} ions into the HAP structure even with a low concentration ($y = 0.005$) results in a sharp enhancement of electron spin relaxation of the NO_3^{2-} radical. The described effect is observed in the whole temperature range. The measured temperature dependences of the spin-lattice relaxation rate T_1^{-1} have a rather complex shape characterized by the sum of various contributions [28–31]; their detailed analysis is beyond the present study.

4. DISCUSSION

NO_3^- and CO_3^{2-} anions are isoelectronic particles ($24e^-$) with molecules identically shaped as a plane triangle (space group D_{3h}). The differences in ion charges

Times of the spin-spin T_2^* and spin-lattice T_1 relaxation of NO_3^{2-} nitrate ions at $T = 300$ K depending on impurity composition of the studied nanoscale hydroxyapatite powders

Sample	T_2^* , ns	T_1 , μs
$\text{Ca}_{10}(\text{PO}_4)_6(\text{OH})_2$	5330(40)	20(1)
$\text{Ca}_{9.5}\text{Na}_{0.5}(\text{PO}_4)_{5.5}(\text{CO}_3)_{0.5}(\text{OH})_2$	5330(15)	19(2)
$\text{Ca}_{9.995}\text{Mn}_{0.005}(\text{PO}_4)_6(\text{OH})_2$	155(6)	1.0(3)

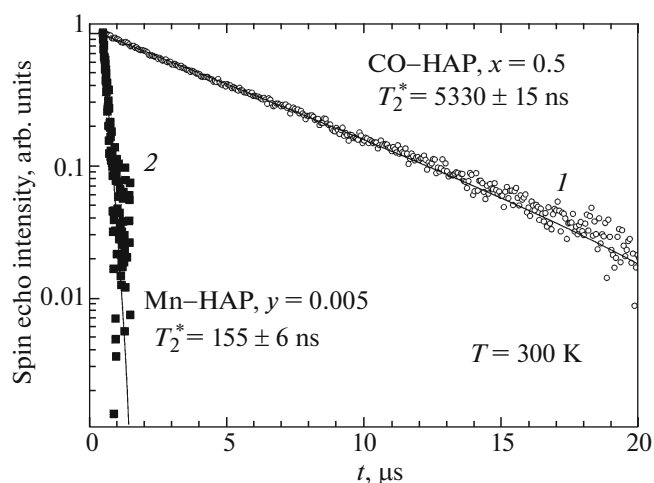


Fig. 2. Effect HAP sample codoping with manganese and carbonate ions on transverse magnetization decay for nitrate ions at $T = 300$ K and their corresponding monoexponential approximations with shown times T_2^* : (1) CO-HAP sample, $T_2^* = 5330 \pm 15$ ns; (2) Mn-HAP sample, $T_2^* = 155 \pm 6$ ns. The data are presented on the semilogarithmic plot.

and sizes (thermochemical radii are 1.89 and 1.85 Å, respectively) mean that the electrostatic interaction of the nitrate anion with calcium cations is weaker than the $\text{Ca}^{2+} \leftrightarrow \text{CO}_3^{2-}$ interaction. This means that the trend toward the occupation of the hexagonal channel in the HAP structure (the so-called *A*-site) for the nitrate anion, characterized by high positive charge density, is less pronounced than for the carbonate ion. Chemically, this corresponds to that the anion alkalinity decreases in the row $\text{OH}^- > \text{CO}_3^{2-} > \text{NO}_3^-$. Indeed, as is shown in our previous studies [16–18], it follows from spectroscopic characteristics of radiation-induced nitrate radicals that they almost immediately substitute the PO_4^{3-} group in HAP crystal structure as their content increases (*B*-type substitution, see Fig. 3). At the same time, carbonate ions can be introduced into the OH-group site (*A*-type substitution) or according to the *B*-type. The effect of HAP doping with carbonate ions with concentrations from 0 to 14 wt % on the intensity of the EPR spectrum of NO_3^{2-} radicals allowed the conclusion that CO_3^{2-} ions are introduced into the HAP structure in the used synthesis process initially according to the *A*-type substitution and then by the *B*-type [16]. At the carbonate ion concentration of ~7 wt %, nitrate ions are almost completely substituted with more alkaline carbonate anions.

Let us consider the case of codoping with manganese ions. The performed EPR and mass spectrometric measurements make it possible to quantitatively

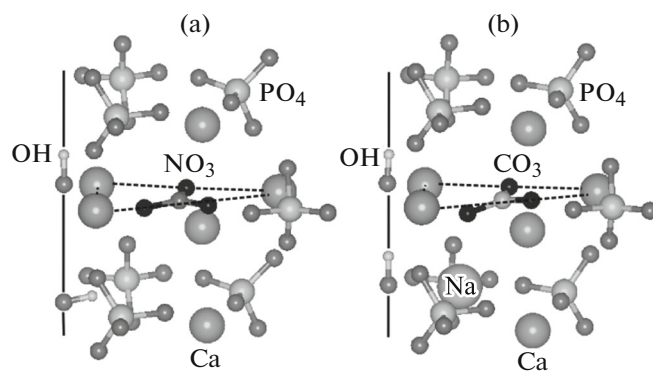


Fig. 3. Hydroxyapatite crystal cells containing (a) nitrate ions and (b) carbonate ions in the case of *B*-type substitution.

estimate the concentration of paramagnetic centers in one nanoparticle (assuming that all manganese ions are in the 2+ state), i.e., no more than two nitrate ions for all studied samples and no more than 50 manganese ions at $y = 0.005$ per one spherical nanoparticle 35 nm in diameter. Taking into account the monoexponentiality of the transverse magnetization decay and the longitudinal magnetization restoration curve for all studied samples, it can be expected that there is the tendency toward certain relative positions of $\text{NO}_3^-/\text{NO}_3^{2-}$ and Mn^{2+} impurities in the HAP lattice.

The NO_3^{2-} radical relaxation enhancement is most likely caused by the spin–spin interaction with rapidly relaxing Mn^{2+} ions distributed near impurity nitrate. To simplify the analysis, we considered the simplest cases of pairs of interacting paramagnetic centers arranged at the fixed distance $r_{\text{N-Mn}}$ corresponding to the interatomic distance in the HAP lattice in the case of the isovalent substitution of various Ca sites with manganese.

It is accepted to distinguish two main components of the spin–spin interaction: dipolar and scalar (exchange) ones. In this case, the exchange mechanism dominates at relatively small distances between paramagnetic centers. Indeed, an analysis of the exchange interaction value determined based on the results of DFT + *U* numerical calculations shows that the constant J_{ex} is 1.72 meV (415.89 GHz) and 0.02 meV (4.84 GHz) in magnitude for configurations with interatomic distances $r_{\text{N-Mn}} = 0.34$ and 0.63 nm, respectively, and exceeds the dipole interaction value (1.32 and 0.21 GHz in the point-dipole approximation). At the same time, the value of J_{ex} calculated for the configuration with $r_{\text{N-Mn}} = 0.85$ nm is less than 10^{-3} meV, which is lower than the accuracy of calculated energies of the system ground state. Hence, beginning approximately with this distance, the dominant contribution of the dipole mechanism should appear.

The effect of the dipole interaction on the NO_3^{2-} radical relaxation enhancement can be estimated according to the theory presented, e.g., in [32, 33]. This makes it possible to estimate $r_{\text{N-Mn}}$ as

$$r_{\text{N-Mn}}^6 [\text{m}^6] = 8.4 \times 10^{-54} / \Delta(1/T_1) T_{2\text{Mn}}, \quad (3)$$

where $\Delta(1/T_1) = 1/T_1 - 1/T_{1i}$ is the enhancement of the longitudinal spin relaxation of the NO_3^{2-} radical by a single Mn^{2+} ion; T_{1i} and T_1 are the relaxation times obtained, respectively, for the case of the isolated NO_3^{2-} radical (in the absence of metal ions) and in the system containing an impurity Mn^{2+} ion; and $T_{2\text{Mn}}$ is the time of transverse relaxation of the Mn^{2+} ion. In deriving formula (3), it was taken into account that the metal ion g -factor is close in magnitude to the radical g -factor. Furthermore, it is accepted that the relaxation characteristics were obtained in the experiment at a magnetic field corresponding to the perpendicular orientation of the NO_3^{2-} radical.

The calculation by formula (3) shows that the distance $r_{\text{N-Mn}}$ is less than 5 nm. From this approximate estimate, it necessarily follows that interacting NO_3^{2-} and Mn^{2+} centers appear localized within one nanoparticle in the case of HAP codoping with nitrate and manganese ions (the average size of the samples under study is 35 ± 15 nm). Thus, a relatively simple measurement of relaxation times directly indicates the possibility of nanoparticle codoping by various paramagnetic impurities.

The results obtained show that the NO_3^{2-} radical should be affected by the set of impurity Mn^{2+} ions distributed in its spatial proximity. As a consequence, the time evolution of the spin echo of the NO_3^{2-} paramagnetic center should be controlled by the superposition of all possible relative orientations of paramagnetic centers, which significantly complicates a more detailed analysis.

5. CONCLUSIONS

The use of the approach based on measurements of spectroscopic and relaxation characteristics of the paramagnetic centers allowed us to reveal the tendency of Mn^{2+} ions and oppositely charged nitrogen impurities toward localization in the spatial proximity within HAP nanocrystals. This is the first experimental observation of the interaction of oppositely charged impurity ions in the HAP structure at the atomic level. By the example of nanoscale HAP powders, it was shown that various EPR approaches can be efficient tools for studying anion and cation (co)doping of nanocrystals.

The energy advantage of codoping can also be expected in the case of introduction of other anionic

impurities. In turn, this should directly affect functional properties of materials. We expect that the shown capabilities of modern EPR spectroscopy methods can and should be efficiently used in the study of synthesis of functional (nano)materials with predetermined properties.

ACKNOWLEDGMENTS

This study was performed within a budget financing project and the program of increasing the Kazan Federal University competitiveness. E.S. Klimashina and V.I. Putlyaev acknowledge the support of the Russian Foundation for Basic Research (projects nos. 15-08-99597 and 15-03-09387); equipment purchased within the Moscow University Development program was used.

REFERENCES

1. A. A. Kaminskii and B. M. Antipenko, *Multilayer Functional Schemes of Crystal Lasers* (Nauka, Moscow, 1989) [in Russian].
2. M. Laroche, S. Girard, R. Moncourage, M. Bettinelli, R. Abdulsabirov, and V. Semashko, *Opt. Mater.* **22**, 147 (2003).
3. A. S. Nizamutdinov, V. V. Semashko, A. K. Naumov, S. L. Korableva, R. Yu. Abdulsabirov, A. N. Polivin, and M. A. Marisov, *J. Lumin.* **127**, 71 (2007).
4. S. V. Dorozhkin, *Am. J. Biomed. Eng.* **2**, 48 (2012).
5. A. B. Brik, A. P. Shpak, V. L. Karbovskii, A. P. Klimenko, V. A. Dubok, A. M. Kalinichenko, N. N. Bagmut, and V. V. Bevz, *Mineral. Zh.* **27**, 5 (2005).
6. J. Hui and X. Wang, *Inorg. Chem. Front.* **1**, 215 (2014).
7. M. Islam, P. C. Mishra, and R. Patel, *J. Environ. Manage.* **91**, 1883 (2010).
8. *Biomedical Engineering—Frontiers and Challenges*, Ed. by R. Fazel-Rezai (InTech, Rijeka, Croatia, 2011), p. 75.
9. S. H. Chu, D. F. Feng, Y. Ma, and Z. Q. Li, *Int. J. Nanomed.* **7**, 3659 (2012).
10. M. Iafisco, J. M. Delgado-Lopez, E. M. Varoni, A. Tampieri, L. Rimondini, J. Gomez-Morales, and M. Prat, *Small* **9**, 3834 (2013).
11. R. Gibson and W. Bonfield, *J. Biomed. Mater. Res.* **52**, 697 (2002).
12. M. P. Moreira, V. T. Da Silva Aragão, G. DeAlmeida Soares, and E. A. Dos Santos, *Key Eng. Mater.* **493–494**, 20 (2012).
13. B. V. Yavkin, G. V. Mamin, S. B. Orlinskii, M. R. Gafurov, M. Kh. Salakhov, T. B. Biktagirov, E. S. Klimashina, V. I. Putlayev, Y. D. Tretyakov, and N. I. Silkin, *Phys. Chem. Chem. Phys.* **14**, 2246 (2012).
14. M. R. Gafurov, B. V. Yavkin, T. B. Biktagirov, G. V. Mamin, S. B. Orlinskii, V. V. Izotov, M. Kh. Salakhov, E. S. Klimashina, V. A. Abdulyanov, I. M. Ignatjev, R. N. Khairullin, A. V. Zamochkin, and Y. A. Chelyshev, *Magn. Reson. Solids* **15**, 13102 (2013).
15. T. B. Biktagirov, Y. A. Chelyshev, M. R. Gafurov, G. V. Mamin, S. B. Orlinskii, Y. N. Osin, and

- M. Kh. Salakhov, *J. Phys.: Conf. Ser.* **478**, 012002 (2013).
16. T. Biktagirov, M. Gafurov, G. Mamin, E. Klimashina, V. Putlayev, and S. Orlinskii, *J. Phys. Chem. A* **118**, 1519 (2014).
17. M. Gafurov, T. Biktagirov, B. Yavkin, G. Mamin, Y. Filippov, E. Klimashina, V. Putlayev, and S. Orlinskii, *JETP Lett.* **99** (4), 196 (2014).
18. T. B. Biktagirov, M. R. Gafurov, G. V. Mamin, S. B. Orlinskii, B. V. Yavkin, A. A. Rodionov, E. S. Klimashina, V. I. Putlyaev, and Ya. Yu. Fillipov, *Opt. Spectrosc.* **116** (5), 715 (2014).
19. M. Gafurov, T. Biktagirov, G. Mamin, and S. Orlinskii, *Appl. Magn. Reson.* **45**, 1189 (2014).
20. L. G. Gilinskaya and M. Ya. Shcherbakova, in *Physics of Apatite*, Ed. by V. S. Sobolev (Nauka, Novosibirsk, 1975), pp. 7–63 [in Russian].
21. P. Fattibene and F. Callens, *Appl. Radiat. Isot.* **68**, 2033 (2010).
22. J. A. Weil and J. R. Bolton, *Electron Paramagnetic Resonance: Elementary Theory and Practical Applications*, 2nd ed. (Wiley, Hoboken, New Jersey, 2004).
23. J. P. Perdew, K. Burke, and M. Ernzerhof, *Phys. Rev. Lett.* **77**, 3865 (1996).
24. D. Vanderbilt, *Phys. Rev. B: Condens. Matter* **41**, 7892 (1990).
25. H. J. Kulik, M. Cococcioni, D. A. Scherlis, and N. Marzari, *Phys. Rev. Lett.* **97**, 103001 (2006).
26. P. Giannozzi, S. Baroni, N. Bonini, M. Calandra, R. Car, C. Cavazzoni, D. Ceresoli, G. L. Chiarotti, M. Cococcioni, I. Dabo, A. Dal Corso, S. Fabris, G. Fratesi, S. de Gironcoli, R. Gebauer, et al., *J. Phys.: Condens. Matter.* **21**, 395502 (2009).
27. E. Ruiz, J. Cano, S. Alvarez, and P. Alemany, *J. Comput. Chem.* **20**, 1391 (1999).
28. A. Abragam and B. Bleaney, *Electron Paramagnetic Resonance of Transition Ions* (Oxford University Press, Oxford, England, 1970), p. 541.
29. L. K. Aminov, V. A. Ivanshin, I. N. Kurkin, M. R. Gafurov, I. Kh. Salikhov, H. Keller, and M. Gutmann, *Physica C (Amsterdam)* **349**, 30 (2001).
30. M. R. Gafurov, L. K. Aminov, I. N. Kurkin, and V. V. Izotov, *Supercond. Sci. Technol.* **18**, 352 (2005).
31. H. Sato, B. A. Filas, S. S. Eaton, and G. R. Eaton, *Radiat. Meas.* **42**, 997 (2007).
32. D. J. Hirsh, W. F. Beck, J. B. Innes, and G. W. Brudvig, *Biochemistry* **31**, 532 (1992).
33. A. V. Kulikov and G. I. Likhtenstein, *Adv. Mol. Relax. Interact. Processes* **10**, 47 (1977).

Translated by A. Kazantsev